EFDA–JET–CP(14)01/21

A. Scarabosio, T. Eich, F. Hoppe, I. Paradela, B. Sieglin, F. Reimold,
M. Rack, M. Groth, M. Wischmeier, G. Arnoux, I. Balboa, S. Marsen,
the ASDEX Upgrade Team and JET EFDA contributors

Scaling of the Divertor Power Spreading (S-factor) in Open and Closed Divertor Operation in JET and ASDEX Upgrade

"This document is intended for publication in the open literature. It is made available on the understanding that it may not be further circulated and extracts or references may not be published prior to publication of the original when applicable, or without the consent of the Publications Officer, EFDA, Culham Science Centre, Abingdon, Oxon, OX14 3DB, UK."

"Enquiries about Copyright and reproduction should be addressed to the Publications Officer, EFDA, Culham Science Centre, Abingdon, Oxon, OX14 3DB, UK."

The contents of this preprint and all other JET EFDA Preprints and Conference Papers are available to view online free at www.iop.org/Jet. This site has full search facilities and e-mail alert options. The diagrams contained within the PDFs on this site are hyperlinked from the year 1996 onwards.

Scaling of the Divertor Power Spreading (S-factor) in Open and Closed Divertor Operation in JET and ASDEX Upgrade

A. Scarabosio[1], T. Eich[1], F. Hoppe[1], I. Paradela[1], B. Sieglin[1], F. Reimold[1], M. Rack[2], M. Groth[3], M. Wischmeier[1], G. Arnoux[4], I.Balboa[4], S. Marsen[5], the ASDEX Upgrade Team[1] and JET EFDA contributors*

JET-EFDA, Culham Science Centre, OX14 3DB, Abingdon, UK

[1]Max-Planck-Institut für Plasmaphysik, Boltzmannstr 2., D-85748 Garching, Germany
[2]Institute of Energy and Climate Research-Plasma Physics, Forschungszentrum Jülich GmbH, Association EURATOM-FZJ, Partner in the Trilateral Euregio Cluster, D-52425 Jülich, Germany
[3]Aalto University, Association EURATOM-Tekes, Espoo, Finland
[4]EURATOM-CCFE Fusion Association, Culham Science Centre, OX14 3DB, Abingdon, OXON, UK
[5]Max-Planck-Institute for Plasma Physics, Wendelsteinstr.1, 17491 Greifswald, Germany
** See annex of F. Romanelli et al, "Overview of JET Results", (24th IAEA Fusion Energy Conference, San Diego, USA (2012)).*

Preprint of Paper to be submitted for publication in Proceedings of the 21st International Conference on Plasma Surface Interactions, Kanazawa, Japan 26th May 2014 - 30th May 2014

ABSTRACT

An experimental database of the power spreading into the target private flux region (S-factor) from ASDEX Upgrade and JET outer target data has been gathered and analysed. The power spreading, combined with the Scrape-Off Layer heat flux decay length λ_q, determines the power exhaust channel width at the divertor target. In terms of main plasma parameters, we find that the poloidal magnetic field plays a major role $S \sim B_{pol}^{-1}$ in both L-mode and H-mode plasmas, similarly to λ_q. Combining JET and AUG data in H-mode with open divertor we obtain a strong and beneficial major radius dependency and no plasma density influence is found. For closed AUG divII configurations in L-mode, however, larger upstream ne clearly broadens S. Interestingly, the scaling of S with divertor parameters, reveals that only target T_e is needed to account for its variation. SOLPS simulations with fixed perpendicular transport reproduce most of the observed phenomenology, suggesting that the observed larger S in closed versus open divertor configuration is simply due to different target T_e generated by larger parallel gradients.

1. INTRODUCTION

Most of the $P_{SOL} \sim 100$MW of power crossing the separatrix at $Q_{DT} = 10$ in ITER will flow inside a narrow channel on open field lines in the scrape-off layer (SOL) connecting directly to the divertor target plates. ITER will ultimately operate in (partial) detached regime but phases with attached divertor plasmas cannot be avoided (i.e. at L-H transition, loss of density or radiation control). Recent work, on attached plasmas, obtained through a multimachine coordinated effort (JET, DIII-D, ASDEX Upgrade (AUG), C-Mod, NSTX and MAST) clear evidence of narrowing of the channel width with the poloidal magnetic field and suggests a very narrow power decay length $\lambda_q \sim 0.63 \cdot B_{pol}^{-1.19} \sim 1$mm for ITER [1]. This result was obtained by fitting the target profile from thermography with the convolution of an exponential function with decay λ_q and a gaussian of width S, due to a residual radial diffusion in the divertor (see section 1.1). For a given total target power P_{tar}, the peak heat flux (q_{max}) will depend also on S, the so called power spreading.

Basically, all recent efforts have focused on the determination of λ_q and the characterisation of S is still largely to be done. We intend here to carry out a first step in this direction and toward the determination of S in future devices also in view of high density operation (divertor plasma detachment). In this work we first study the plasma parameters and geometrical dependencies of S in ASDEX Upgrade and JET under attached divertor conditions starting with type-I ELMy H-Mode plasmas. The analysis of AUG L-mode plasmas identify an important role for the upstream density. Discharges with only intrinsic impurities are considered (no seeding). When available, we explore the connection between divertor variables and target heat fluxes. In the second part, an extensive set of simulations with the SOLPS code package [2] is compared with main experimental finding to validate the physics model therein and to gain insight in the underlying physical processes.

1.1 EXPERIMENTAL ESTIMATION OF THE POWER FALL-OFF WIDTH AND POWER SPREADING FACTOR S

The analysis of measured target profiles in the outer divertor of each machine follows the approach

introduced in [3] which is summarized in the remainder of this section. The SOL power decay length is determined by analysis of heat flux profiles measured at the outer divertor target by means of infrared thermography and/or Langmuir probes. Details of the experimental setup for JET can be found in [4] and for AUG in [5]. Expressing the target coordinate as s and the strike line position on target as s_0 we describe the heat load profile at the divertor entrance as a purely exponential radial decay (characterized by λ_q) $q_{||}(\bar{s}) = q_0 \cdot \exp(\frac{\bar{s}}{\lambda_q})$ and $\bar{s} = s - s_0$, $s \geq s_0$. This exponential profile at the divertor entrance [6], is then diffused radially while travelling towards the target [7]. This process is approximated by a convolution of the exponential profile with the Gaussian function with the width S which we refer to as power spreading parameter and which is assumed to depend on divertor plasma parameters but constant along field lines. Neglecting the flux expansion f_x, the target heat flux profiles are thus expressed as ($\bar{s} \in [-\infty,\infty]$)

$$q(\bar{s}) = \frac{q_0}{2} \exp\left(\left(\frac{S}{2\lambda_q}\right)^2 - \frac{\bar{s}}{\lambda_q}\right) \cdot \mathrm{erfc}\left(\frac{S}{2\lambda_q} - \frac{\bar{s}}{S}\right) + q_{BG} \tag{1}$$

with q_{BG} the background heat flux. The experimental profiles can be well described by numerical least-squares fits according to (1) with the free parameters S, λ_q, q_0, qBG and s_0 as shown in [1,9,10] for several tokamaks and plasma regimes. The same fitting technique can be applied to simulated heat fluxes from SOLPS (on a typical grid of 18×48 cells) to extract λ_q and S. The quality of the fit is generally very good as shown in Figure 1. Another quantity of interest is the so called integral power decay length [11] defined as

$$\lambda_{int} = \frac{\int (q(\bar{s}) - q_{BG}) d\bar{s}}{q_{max}} \tag{2}$$

and relating the maximum peak heat flux q_{max} and the deposited power, a crucial design parameter for the power handling capabilities of a large device such as ITER. Within the framework model of Eq.1, the relation between exponential and integral decay lengths can be written with good approximation as [12]

$$\lambda_{int,model} \simeq \lambda_q + 1.64S \tag{3}$$

It should be noted that any physical study of the SOL power decay length should use λ_q and not λ_{int} as done in earlier attempts [11,13], the latter having a stronger dependence on the divertor physics through S as seen in (3). For instance attempts to regress the data would lead to different results if using λ_q or λ_{int}. Instead, λ_q and S have to be analysed separately. As already mentioned, in references [1,3,9] an extensive treatment of λ_q has been presented leading to the 1mm prediction for ITER. It becomes clear that a value of S larger than this would dominate over λ_q when determining λ_{int}, and therefore an extrapolation of S to ITER is desirable. A first step toward such extrapolation is described in the remainder of the paper based on experimental data analysis and theoretical model validation.

2 SCALING OF S IN AUG AND JET PLASMAS

2.1 THE EXPERIMENTAL DATABASES

We analyse data from JET and AUG H-mode plasmas with carbon target. For JET we only use data in tile 5 configuration (horizontal target) whereas for AUG we both include data with divI configuration (horizontal target) and divIIb configurations (vertical target). More recent AUG L-mode data with divertor IId and divertor III [14] is also analysed separately. This choice is dictated mainly by the availability of consistent sets of discharges with similar configuration. Although not representative of all conditions, it covers various combination of divertor geometry and target material as well as a large range of plasma parameters as summarised in table 1 for each data set. The definition of various parameters in table 1 are I_p for plasma current, B_{tor} for toroidal magnetic field, q_{95} for the safety factor at 95% of the poloidal flux, P_{SOL} for power crossing the separatrix, for plasma triangularity, n_p for plasma density, κ for plasma elongation and B_{pol} for the poloidal magnetic field at the outer midplane separatrix. The important geometrical parameters such as the minor radius a and the major radius R_{GEO} are taken to be $(R_{GEO},a) = (2.95,0.95)$ and $(1.65,0.51)$ m for JET and AUG, respectively. Different divertor plasma conditions are included, ranging from fully attached low recycling in H-mode and L-mode with peak target temperature of around 45-50eV to high recycling L-mode with target temperature of ~10eV.

2.2 REGRESSION FOR H-MODE PLASMAS

For H-mode plasmas it was showed that λ_q scales primarily with the poloidal magnetic field as $\lambda_q \sim 0.68 \cdot B_{pol}^{-1.07}$ [1]. No statistically relevant dependency on major R_{geo} as well as input power dependency was found. Interestingly, both horizontal and vertical target data were included in the same regression with no obvious data separation (i.e. no geometry effect). The situation for the spreading parameter S appears to be different. Comparing AUG horizontal (only 6 discharges) and vertical target data one finds $< S_{divII} > = < S_{divI} > \sim 3.5$, whereas $< \lambda_{q,divII} > = < \lambda_{q,divI} > \sim 1.25$ [1]. This large difference indicates a strong sensitivity on divertor geometry. Since S is thought to represent the heat flux leakage into the divertor private flux region, it is thus plausible that the divertor geometry may have a strong influence. From the point of view of an empirical regression, including divII data would lead to a strong and negative scaling of S with R_{GEO}. Standard arguments suggest that this is unlikely (i.e. larger connection length $l \propto R$ with larger R_{geo}). For the moment, we thus exclude this data from the regression and use only horizontal target data. The important issue of the geometry effect will be addressed through simulations and presented in section 3.2. Here we concentrate on plasma parameter dependencies. We use plasma and machine parameters in table 1 and employ standard numerical tools for multivariate regression, using power law of the form $S/f_x = C \cdot X^x Y^y Z^z$, etc, with fx the flux expansion [3] and C a constant. We use the multiple (squared) correlation coefficient R^2 as fit qualifier. In Figure 2 we show the best regression giving us

$$S_{H-mode}\,(\mathrm{mm}) = (0.12 \pm 0.07) P_{SOL}^{0.21 \pm 0.11} n_p^{-0.02 \pm 0.23} B_{pol}^{-0.82 \pm 0.27} R_{GEO}^{0.71 \pm 0.50}. \qquad (4)$$

As for λ_q, the driving parameter is the poloidal magnetic field but with now a strong dependence on R_{GEO}. Although still uncertain, a R_{geo} dependence may be connected with the standard divertor physics picture of longer connection length which allows more transport (radial and parallel) to occur on the way toward the target plate. Only weak P_{SOL} and basically no density as well as B_{tor} (not shown) dependence is found. The strong variation with Bpol may have two main origins: one direct, due to changes in the radial transport (i.e. $\chi_\perp(B_{pol})$), and one indirect through λ_q which is setting the heat flux channel width at the divertor entrance thus influencing the divertor plasma parameters. Just as an exercise, we plug the ITER parameters of table 1 with a = 2.0 and R_{GEO} = 6.2m into eq. (2) to get S ~ 1mm. As known, ITER adopted a closed divertor geometry and, fortunately, this extrapolation is likely to be strongly underestimating the true value. For a more realistic estimation a set of JET data with vertical target is of crucial importance.

2.3 REGRESSION FOR L-MODE PLASMAS

A set of dedicated L-Mode discharges have been conducted in ASDEX-Upgrade with divIId in deuterium and hydrogen. The plasma density was varied to span from very low to high divertor recycling conditions. The analysis of these experiments revealed an increase of both λ_q and S with n_e [9,15] which was not observed in previous work [10]. It was shown that a good quality regression in L-mode is given by $S = 0.09 n_{e,edge}^{1.02} B_{pol}^{1.01}$ thus showing the usual poloidal field dependence, a linear positive trend with plasma density (here the edge electron density ne;edge is used but a similar result is obtained with core or volume averaged density) and no difference between hydrogen isotopes. We have recently increased the L-mode database adding data from the newly installed full-W divertor III [14] (Figure 3). As expected from the minor changes, the new data is consistent with the older within error bars, as shown in Figure 3. So far we have studied and expressed S in terms of main plasma parameters. But S originates in the divertor and thus a direct dependency on divertor plasma parameters is expected. We have tested S against T_e and n_e at the target from Langmuir probe data and the neutral flux density Γ_D measurements from below the divertor dome, a good proxy for the divertor neutral density and recycling strength [16]. The result is plotted in Figure 4. It can be seen (for the case of (T_e, Γ_D)) that the target Te alone can represent the data quite satisfactorily. It is interesting and perhaps surprising that only one divertor parameter can equally well explain the dependency on the upstream variables (n_p, B_{pol}). This latter result simply confirms that S is a divertor effect and thus it depends on divertor parameters and geometry. With this in mind, it may be easier to believe that present plasma edge theoretical models, such as the one in SOLPS, are more likely to explain the observations on S than on q, that is more strongly connected to anomalous radial transport in the upstream SOL. In fact, we will see in the remainder of the paper that the observed important relation $S(T_{e,tar})$ is reproduced by SOLPS.

3. SOLPS CHARACTERISATION OF TARGET HEAT FLUX PROLE

An very extensive set of plasma edge simulations has been performed in order to: i) compare quantitatively the predicted heat flux characteristics (power spreading S in particular) with experiments, ii) improve understanding of the physical mechanisms behind major scaling parameters,

iii) facilitate scaling and extrapolation toward new devices and divertor configurations. We used the SOLPS (version 5.0) code package which consists mainly of B2.5, a 2D multi-fluid plasma edge code [17] solving Braginskii-like equations, coupled to EIRENE [18], a 3D Monte-Carlo code assessing the effect of neutrals. A diffusive radial transport model with radially and poloidally varying anomalous coefficients $\chi_\perp$ and $D_\perp$ is implemented into SOLPS. L-mode like plasmas are generated by setting appropriate transport coefficients and input power. Fine tuning of such parameters typically allows to match upstream experimental profiles. The code is run without cross-field drifts activated hence the analysis focuses on the outer target only [19]. The resulting heat flux profile is analysed and fitted with the same function used for the experimental profiles (see examples in Figure 1). The simulations were executed mainly on two grids: based on the same magnetic equilibrium of AUG Pulse No: 21303 one grid uses the vertical target geometry of divIIb (closed divertor configuration), on the second we replaced the divertor structures with the older divI (open configuration) featuring an outer horizontal target plate with otherwise identical setup described in [20] and references therein. The physical domain discretisation for the two cases is depicted in Figure 5. By doing so we can exclude the effects of subtle difference in the magnetic equilibrium and grids that may mask the true geometrical effect. The wall and target material is carbon which constitutes the main impurity with traces of helium. A rough validation against the AUG L-mode ohmic Pulse No: 21303 was chosen as starting point with the purpose of generating a plasma solution with the relevant conditions. Upstream conditions are well matched and the target ones within a factor of three or better (see [15]). Then, scans of separatrix upstream density at LFS midplane, input power, transport coefficients, particle throughput and pitch angle are used to systematically extract the dependence of the target heat fluxes and S in particular. We have also varied the numerical model within SOLPS by changing target sputtering yield and thus the impurity content as well as divertor geometry. More than 1000 steady-state simulations were executed, spanning various divertor conditions with target separatrix Te ranging from almost 100eV down to 1-2eV for the highest densities with divIIb configuration, thus from the so called sheath-limited regime to high recycling partially detached plasmas. Finally, a density scan based on validated SOLPS solution against the AUG H-mode discharge #28903 [21] has been analysed to check whether major differences arise due to the different simulation and material parameters (i.e. transport coefficients, np and neutral reflection model at targets).

3.1 SCALING OF S WITH MAJOR INPUT PARAMETERS AND COMPARISON WITH EXPERIMENT WITH CLOSED DIVERTOR

In Figure 6 we plot S/f_x versus n_e and P_{in} from SOLPS together with AUG divIId results. There is a relatively good agreement with the experiments despite no attempt was made to 'tune' the simulations in order to match more closely (except for the reference case of Pulse No: 21303 with 0.7MW P_{in}) the upstream profiles. Similar agreement is found for λ_q (not shown). Most notably, the SOLPS transport coefficients were kept constant during the scans and carbon impurity was used in the simulations whereas the first wall material in AUG was tungsten. This good agreement is encouraging and gives confidence on the adequacy of SOLPS to tackle this particular problem. Summarising the results of many runs, S is seen to scale positively with density (Figure 6) and safety factor q (equivalently

with the pitch angle or the connection length) and negatively with input powers with roughly the following power law: $S \propto n_e^{1.75} \cdot q^{0.61} \cdot P_{in}^{-0:83}$. Qualitatively, S displays the same trends as for the power decay length λ_q (not shown). To further explore the physics variables we vary the particle throughput by changing location and efficiency of the absorbing surfaces (effective pumps) by a factor of 10. Although the convergence property of the code was affected, no significant changes in the final numerical solutions are seen. Switching off CX increases the peak heat flux by 10-20%. Only at high n_e when $T_{e,tar,sep} < 5eV$, S is reduced by 30% (whereas λ_q is barely affected) but all trends remain unchanged. The ion-neutrals elastic collision has no relevant effect in our simulations.

3.2 EFFECTS OF DIVERTOR GEOMETRY AND RADIATION

For the same input parameters the target heat flux profiles in the open divI behave quite differently. Heat flux decay length λ_q basically does not vary with n_e and S increases much less rapidly leading, in general, to S_{divII} / S_{divI}. At Pin = 700kW, for instance, S_{divII} / S_{divI} reaches up to 2.6 which is not far from our experimental observation (see section 2). It is suggested that this behaviour is connected with the different radiation pattern of the two configurations and the effect that this has on the divertor T_e drop (see next section). A closed divertor with vertical targets increases radiation losses [17]. The higher radiation is accompanied by higher neutral particle density and recycling and it is believed to originate from the different reflection properties of neutrals at the targets. The horizontal target of divI (or of JET tile 5) tends to reflect the neutrals away from the separatrix and toward the far SOL whereas the vertical target reflects more toward the separatrix. The higher radiation and neutrals density in seen divII simulations leads to a higher power dissipation and larger T_e drop along the separatrix. When defining the dissipation efficiency as $\eta_{diss} = 1 - P_{tar} / P_{div}$ with P_{tar} the total power reaching the outer target and P_{div} the power entering the outer divertor, one can see that divII is two-fold more efficient in dissipating power (not shown). diss;div−II increases strongly with ne and both D and C impurities contribute almost equally (except at low n_e where C radiation dominates). The role of impurity radiation has been further investigated by 'switching off' carbon sputtering at the targets. As consequence C radiation is drastically reduced with typically $P_{rad,C} < 0.1 \cdot P_{rad,D}$. For divII with no-sputtering, only about 10% of the C radiation is replaced by more D radiation, thus only roughly half of the power is radiated (at highest density 92kW in the outer target against 160kW and 66kW for divII and divI respectively with carbon). The radiation is lower but still localised near the separatrix. As expected, up to 50% increase of total power to the outer target is observed (Figure 8, right axis). Perhaps surprisingly however, the n_e dependency of the heat flux profile shape (in terms of S and λ_q) does not change significantly as shown for divII in Figure 8. We can hence conclude that the strength of the impurity radiation strongly affects the peak power to the target but is its localisation, more connected with divertor geometry, that influences the profile width.We note that this is in line with the experimental observation of basically no differences on λ_q and S between JET tile 5 with CFC and ILW targets [9] despite the different divertor radiation level [22].

3.3 CONNECTION BETWEEN TARGET TE AND S

The analysis in section 2.3 shows the link between S and the target temperature. It turns out that also

in SOLPS $T_{e,tar}$ is the best 'ordering' parameter, able to represent quite accurately the variation of S with several variables $S(n_e, P_{in}, q, \text{geometry}) \Rightarrow S(T_{e,tar,sep})$ into a single one. This is demonstrated in Figure 9. Except for the transport coefficients scans, most database (including results from a 3rd grid based on equilibrium of old divI discharge Pulse No: 7888) collapses into a unique curve with small scatter. We stress the fact that here, the temperature variation is achieved at constant $\chi_\perp$ and $D_\perp$ for each set of data (see legend in Figure 9). A simple fit gives $S/f_x = 2.3\pm0.2 \cdot T_{e,tar,sep}^{-0.36\pm0.03}$ mm with $R^2 = 0.98$. Experimental AUG divII and JET tile 5 data is superimposed to the SOLPS results in Figure 9. The experiments are quite consistent (within uncertainties) with the simulations, especially for $T_{e,tar,sep} \geq 20$eV, the well attached condition we are considering here. For lower temperature, larger error is expected since we used for the experiment $T_{e,tar,max}$ in place of $T_{e,tar,sep}$, not easily available, thus overestimating the temperature. It is interesting to note that $T_{e,tar,sep}$ orders data much better than other target quantities (eg. $T_{e,tar,max}$) indicating the strong link of the width S with the plasma dynamics near the separatrix. In fact, Te,tar,sep can be also replaced by the normalised T_e drop from X-point height to target $\Delta T_{e,sep}/T_{e,tar,x-point}$. It is the T_e drop that regulates the evolution of the ne and T_e profiles from X-point to target (i.e. width, peak values, etc...), determining the heat load width. In Figure 9 we also plot SOLPS H-mode data which is very similar to the L-mode one despite the different upstream and target conditions (i.e. larger np and Pin). Hence, within SOLPS, there is no difference in the S dynamic between L-mode and H-mode plasmas.

Under this new light, it is also possible to understand the difference between the open divI and the closed divI. In Figure 10 we plot $T_{e,tar}$ versus the upstream density for a density scan with divII and divI and with/without target sputtering. For the same upstream ne, we find a much larger $\nabla_\parallel T_e$ and lower target Te that drops more rapidly with ne in divII than in divI. A similar result was also obtained in EDGE2D-EIRENE simulation of JET plasmas with horizontal and vertical targets [22]. Moreover, target T_e is weakly affected by the loss of carbon radiation when sputtering is turned off, consistent with its small influence on S and on λ_q (not shown). Thus the differences with divertor geometry in SOLPS are purely the consequence of the different reduction of Te along the field lines. As shown above, for the same $T_{e,tar}$ both divertors give the same S (but not λ_q!) and no other direct geometry effect is observed.

SUMMARY AND DISCUSSION

We have shown that SOLPS simulations either reproduce or are, at least, not in contradiction with most of the experimental observations, namely: i) $S(n_{e,upstream})$ or equivalently $S(T_{e,target})$ dependency for closed divertor configuration (figures 3 and 4), ii) divertor geometry effect leading to $S_{closed-div} > S_{open-div}$, iii) negligible influence of target material on S and λ_q. The crucial result, here, is that we do not have to invoke perpendicular transport changes to (re)produce all these effects. It is found that, except for very low n_p, S is given by the density profile width at the target. This width depends on the Te drop along field lines near the separatrix (induced by radiation, the 2D nature of transport and T_e dependent $\chi_\parallel$ (eg. from classical conductivity)). If this mechanism dominates over radial transport in tokamak outer divertor plasmas, conditions with low radiation/low n_e, target $T_e \geq 10$eV and $S \geq 1.0-1.5$mm are not possible (at $T_e = 10$eV the simple fit of SOLPS data gives, for

reference, S = 1 mm). In ITER with $\lambda_q \sim S \sim 1$mm peak heat fluxes will be excessively high even for short transient without enhanced radiation losses. Experimentally, it is vital to understand whether the target T_e is the only parameter needed to account for the observed phenomenology or if more subtle perpendicular transport effects have to be invoked.

ACKNOWLEDGEMENT

This work was supported by by EURATOM and carried out within the framework of the European Fusion Development Agreement. The views and opinions expressed herein do not necessarily reflect those of the European Commission.

REFERENCES

[1]. T. Eich et al., Nuclear Fusion **53** (2013) 093031 (7pp)
[2]. R. Schneider et al., Contribution to Plasma Physics **46** (1-2):3-191, (2006)
[3]. T. Eich et al., Physical Review Letters **107** (2011),215001.
[4]. T. Eich et al., Journal of Nuclear Materials **415**, S856 (2011).
[5]. A. Herrmann et al., Plasma Phys. Controlled Fusion **44**, 883 (2002).
[6]. P. Stangeby et al., Nuclear Fusion **50**, 125003 (2010).
[7]. A. Loarte et al., Contribution to Plasma Physics **32**, 468 (1992).
[8]. T. Eich et al., Journal of Nuclear Materials **438**, S72 (2013).
[9]. B. Sieglin et al., Plasma Physics and Controlled Fusion **55** (2013), 124039; 28 and PhD thesis, TU Muenchen 2014
[10]. A. Scarabosio et al., Journal of Nuclear Materials **438** (2013) S426S430
[11]. A. Loarte et al., Journal of Nuclear Materials **266–269**, 587 (1999).
[12]. M. A. Makowski, 2012 Physics of Plasmas **19** 056122
[13]. W. Fundamenski et al., 2011 Nuclear Fusion **51** 083028
[14]. A. Herrmann et al., Fusion Engineering and Design **88** (2013) 577 580
[15]. F. Hoppe, Diploma thesis, LMU Muenchen 2013, http://edoc.mpg.de
[16]. A. Scarabosio et al., Journal of Nuclear Materials **390–391** (2009) 494497
[17]. B.J. Braams, Contributions to Plasma Physics, 1996.
[18]. D Reiter et al.,Fusion Science and Technology, 2005.
[19]. L. Aho-Mantila et al., Nuclear Fusion **52** (2012) 103006 (12pp)
[20]. M. Wischmwier et al., Journal of Nuclear Materials 390391 (2009) 250254
[21]. F. Reimold, this conference
[22]. M. Groth et al., Nuclear Fusion **53** (2013) 093016 (11pp)

	Conf.	Gas	I_p	B_{tor}	q_{95}	P_{SOL}	δ	n_p	κ	B_{pol}
Unit	–	–	MA	T	–	MW	–	$10^{19}\mathrm{m}^{-3}$	–	T
JET-C	tile 5	$D_2/H_2/He$	1.5-3.5	1.0-3.2	2.6-5.5	2-12	0.2-0.4	1.9-4.2	1.8	0.2-0.7
AUG-C	divIIb	D_2	0.8-1.2	1.9-2.4	2.6-5.1	2-5	0.1-0.3	3.5-8.7	1.7	0.2-0.5
AUG-C	divI	D_2	1.0-1.2	1.9-3.0	2.6-4.0	2-4	0.1-0.3	3.7-7.2	1.8	0.4-0.5
AUG-W	divIId	D_2/H_2	0.6-1.0	1.4-2.5	3.1-6.8	0.5-1.5	0.1-0.3	0.8-2.2	1.7	0.22-0.37
AUG-W	divIII	D_2	0.5-0.8	2.4-2.5	4.8–8.8	0.5-1.3	0.1-0.2	0.6-1.1	1.7	0.15-0.25
ITER	–	–	15	5.3	3	100	0.44	12	1.8	1.185

Table 1: Overview of the plasma parameter range for each configuration and target material.

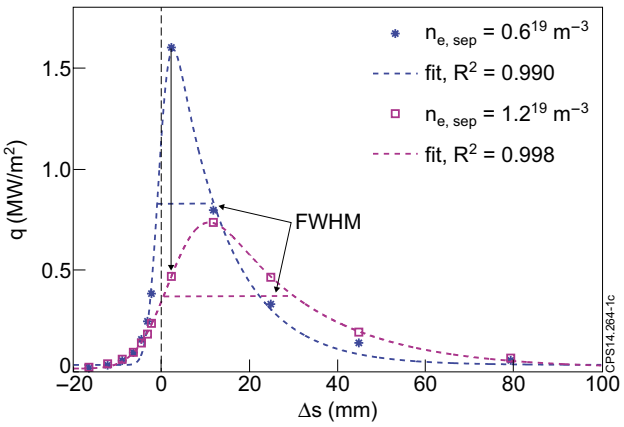

Figure 1: Examples of SOLPS outer target heat flux profiles for divII with relative fit using eq. 1 and for two values of n_p with the same input power. The fit quality is also indicated.

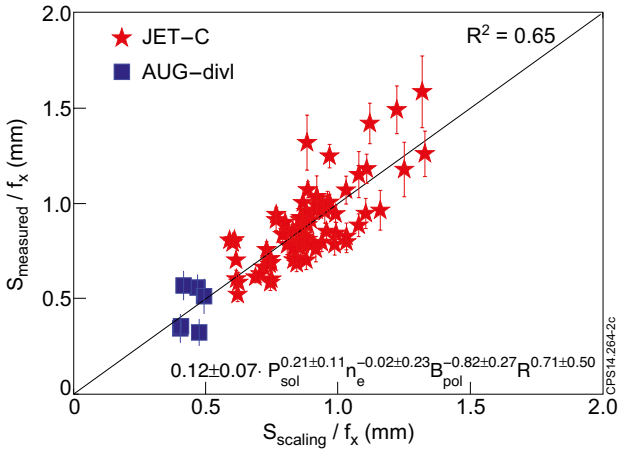

Figure 2: Regression of S for H-mode plasmas in JET and AUG div-I with carbon horizontal target.

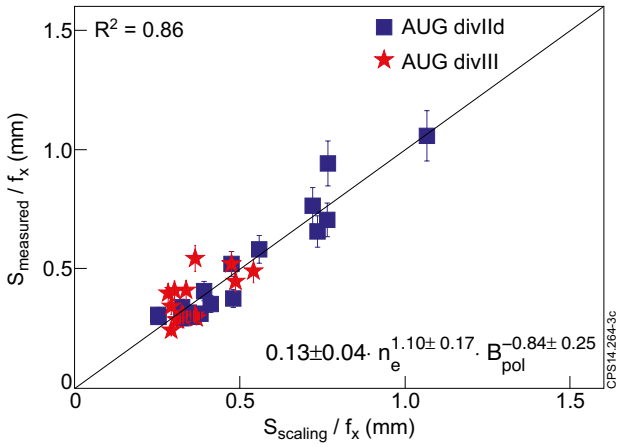

Figure 3: Regression of S for AUG L-mode plasmas with div-IId and div-III vertical W target.

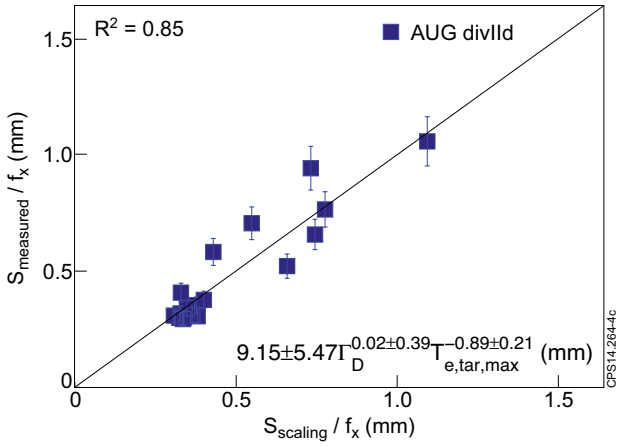

Figure 4: Fit of S for AUG L-mode plasmas with divIId vertical tungsten target with maximum target electron temperature from Langmuir probes.

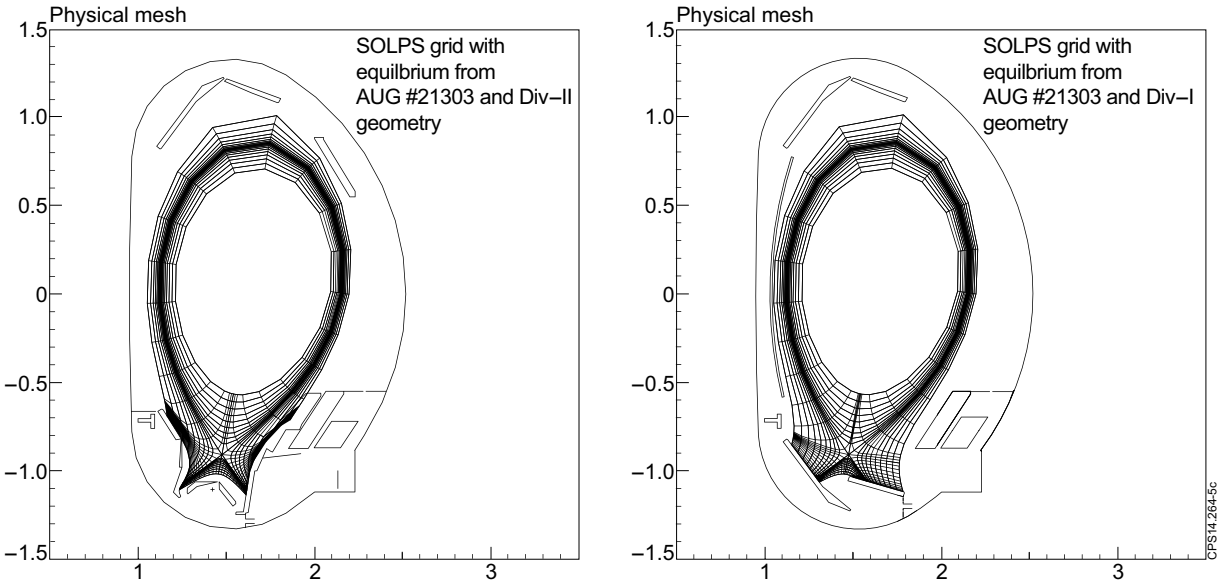

Figure 5: SOLPS grids based on Pulse No: 21303 magnetic equilibrium in closed DivIIb geometry with vertical target (left) and with geometry of the divI featuring a horizontal outer target (right).

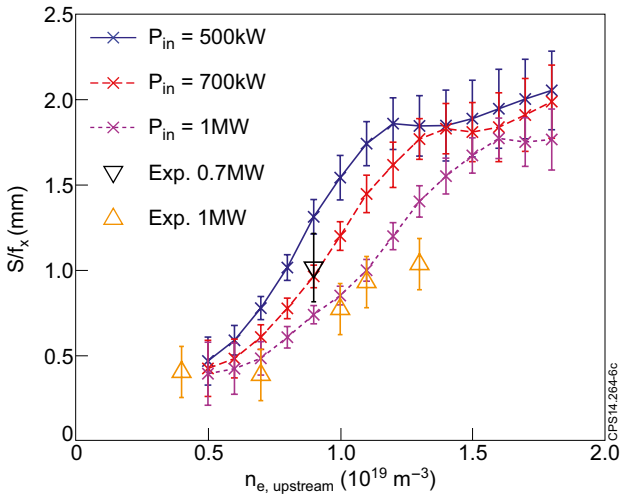

Figure 6: LFS power spreading S/f_x as function of upstream separatrix density and input power with divII configuration compared with AUG L-mode experiments with W targets.

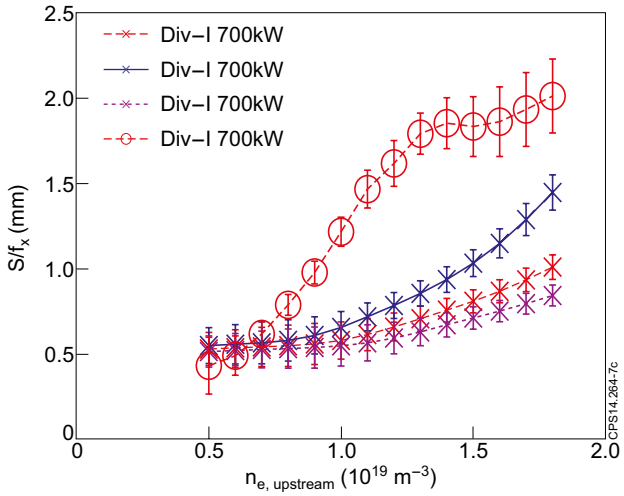

Figure 7: LFS power spreading S/f_x as function of upstream separatrix density and input power for divI configuration. For comparison, S/f_x in divII for P_{in}=700kW is also plotted.

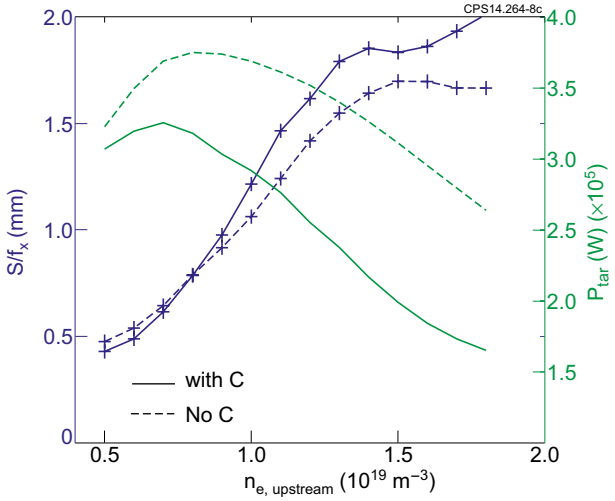

Figure 8: Effect of Carbon impurity in divII simulation at 700kW of input power. Lines with crosses show S for a n_e scan. Dotted lines are for the No C case and the full lines for the C case.

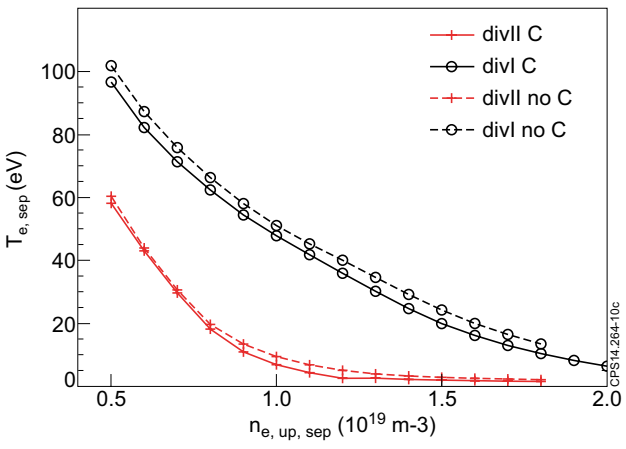

Figure 9: S versus target T_e near the separatrix for most of the numerical database including results from a grid based on old divI Pulse No: 7888. An H-mode density scan is added for comparison as well as experimental data from divIId and JET horizontal target for which maximum target T_e is used instead of $T_{e,tar,sep}$.

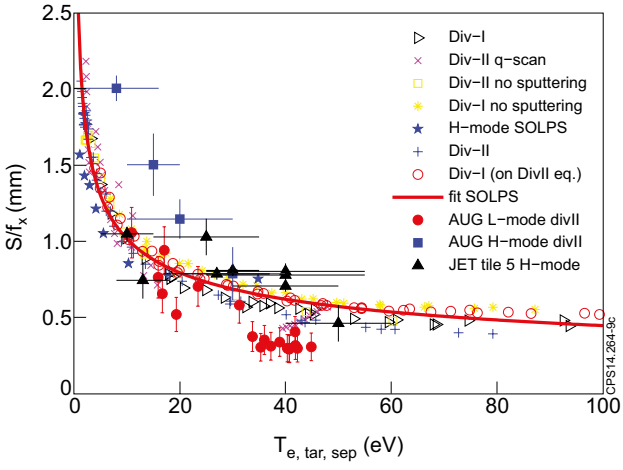

Figure 10: Separatrix target T_e near evolution with upstream separatrix ne for divII (crosses) and divI (circles) with (full line) and without (dashed line) C sputtering.